Enabling Precision Monitoring of Psoriasis Treatment by Optoacoustic Mesoscopy

Authors: Benedikt Hindelang[1,2,3], Teresa Nau[1,2,3], Ludwig Englert[2,3], Andrei Berezhnoi[2,3], Felix Lauffer[1], Ulf Darsow[1], Tilo Biedermann[1], Kilian Eyerich[1], Juan Aguirre[2,3,*], Vasilis Ntziachristos[2,3,4,*]

Affiliations:

[1]Department of Dermatology and Allergy, Technical University of Munich; 81675, Munich, Germany.

[2]Chair of Biological Imaging, Technical University of Munich; 81675, Munich, Germany.

[3]Institute of Biological and Medical Imaging, Helmholtz Zentrum Munich; 85764, Neuherberg, Germany.

[4]Munich Institute of Robotics and Machine Intelligence (MIRMI), Technical University of Munich; 81675, Munich, Germany.

*Corresponding authors. Email: VN bioimaging.translatum@tum.de; JA juanaguir@gmail.com

One Sentence Summary: Optoacoustic imaging can assess psoriasis treatment with unprecedented accuracy having broad implications for drug discovery and precision medicine.

Abstract: Psoriasis is a widespread inflammatory skin disease affecting about 2% of the general population. Recently, treatments that specifically target key pro-inflammatory cytokines driving the disease have been developed to complement conventional therapies with unspecific anti-proliferative or anti-inflammatory effects. Efficient monitoring of treatment efficacy in the context of precision medicine and the assessment of new therapeutics requires accurate non-invasive readouts of disease progression. However, characterization of psoriasis treatment remains subjective, based on visual and palpatory clinical assessment of features observed on the skin surface. We hypothesized that optoacoustic (photoacoustic) mesoscopy could offer label-free assessment of inflammation biomarkers, extracted from three-dimensional (3D) high-resolution images of the human skin, not attainable by other noninvasive methods. We developed a second-generation ultra-broadband optoacoustic mesoscopy system, featuring sub-10 μm resolution and advanced motion correction technology, and performed 80 longitudinal measurements of 20 psoriatic skin plaques in humans under conventional inpatient treatment or receiving biologics with concomitant topical corticosteroid treatment. Optoacoustic image analysis revealed inflammatory and morphological skin features that indicated treatment efficacy with sensitivity, accuracy, and precision that was not possible using clinical metrics. We identify 3D imaging

biomarkers that reveal responses to treatment and offer the potential to facilitate disease and treatment characterization. Our findings suggest that optoacoustic mesoscopy may offer a method of choice for yielding both qualitative and quantitative evaluations of skin treatments that are inaccessible by other methods, potentially enabling optimized therapies and precision medicine in dermatology.

INTRODUCTION

Affecting about 2% of the general population in Europe and North America, psoriasis is a widespread chronic inflammatory skin disease that severely impairs quality of life and financially burdens the healthcare system and society (*1*). The disease is associated with a dysregulation of dendritic cells that produce, among other mediators, Tumour Necrosis Factor alpha (TNFα) and interleukin-23 (IL-23). In particular, the activation of T helper 17 (T_H17) cells, which release interleukin 17 (IL-17), contributes to the inflammation and metabolic activation of the skin. This includes the release of pro-angiogenic vascular endothelial growth factor (VEGF). Phenotypically, histology of psoriatic skin exhibits hyperkeratosis, acanthosis, inflammatory cellular infiltrate and a characteristic modified microvascular architecture. Macroscopically, the skin lesions present as demarcated erythematous plaques with adherent white scales (*1, 2*).

There is no known cure for psoriasis. There is, however, strong interest in developing new treatments for managing the disease and suppressing the symptoms, and several treatment alternatives exist. Treatment is often required for a lifetime, but responses to therapies differ for each patient. Mild cases of psoriasis can be controlled by topical treatments using symptomatic descaling with agents like salicylic acid and broadly anti-proliferative and anti-inflammatory drugs, such as corticosteroids, dithranol and vitamin D derivatives, which modulate the local immune response and keratinocyte proliferation. Non- or mild-responders to topical treatment may additionally require the administration of phototherapy or systemic drugs. Narrow-band Ultraviolet B (NB-UVB) phototherapy and psoralen-UVA (PUVA) photochemotherapy modulate inflammation by suppressing, among other effects, the Th17 inflammatory pathway (*3*). While topical treatment and phototherapy are effective in most cases, they are time consuming and cannot be administered indefinitely. Conventional systemic therapies include methotrexate, acitretin, ciclosporin A, and fumaric acid esters, which non-specifically target proinflammatory and proliferative pathways and are efficient in up to 50% of patients (*2*). Patients suffering from moderate to severe psoriasis who are treated with conventional therapies may experience recurrent relapses, repeatedly requiring expensive inpatient care. The introduction and ongoing development of biologics in recent years, mostly monoclonal antibodies targeting proinflammatory cytokines, such as TNFα (Infliximab), IL-17 (Iexkizumab, Brodalumab, Secukinumab) or IL-23 (Ustekinumab, Guselkumab), has revolutionized the treatment of patients for whom conventional approaches have failed, were contraindicated, or were not tolerated. Biologics are very effective with, for example, IL 17-inhibitors reducing disease severity by as much as 90% in about 70% of patients (*2, 4*). Biologics are also safe and do not exhibit relevant cumulative toxicity or drug–drug interactions. However, biologics treatments are about 10 times more expensive than conventional treatments (around 15 000-25 000 € per year), which has largely restricted their role to second-line therapies (*2*).

Research into novel therapeutics and optimization of treatment requires accurate, precise, and longitudinal assessment of disease severity on an individualized basis. Ineffective therapies must be recognized, adapted, or changed as early as possible to avoid further disease progression and excessive treatment costs. Adapting, for example, the frequency of biologics administration to the patient's response could make these therapies more cost efficient. To fulfil the promise of personalized medicine, such evaluations require objective and quantitative grading methods. Given the strong interest in developing new psoriasis drugs, especially biologics, such grading methods are urgently needed to assess the efficacy of new therapeutics. In particular, a non-invasive method for assessing psoriasis would be highly desirable since the current gold-standard of histology is inappropriate for longitudinal measurements. Disease severity is usually graded and monitored over time using clinical scores such as the psoriasis severity index (PASI), which is calculated from the percentage of affected body surface, redness (erythema), thickness (induration), and scaling of the psoriatic plaque as graded by visual and palpation assessment. The local PASI (or plaque PASI) is an alternative index that does not take into account the percentage of affected body and is used to monitor changes in psoriasis severity at a single location, for example at a single psoriatic plaque (*5*).

Despite the acceptance of the PASI or local PASI as disease severity metrics, palpatory and visual inspection is inherently subjective, offers only a surface view of the skin condition, has low sensitivity to capturing subtle changes in mild disease, and cannot assess or quantify critical pathological features within the skin (*6*). As an alternative we consider herein ultra-broadband raster-scan optoacoustic mesoscopy (UB-RSOM) to resolve detailed 3D images psoriatic skin under treatment and investigate how skin microvasculature and other skin features relate to treatment response. Microvascular changes are increasingly being identified as important pathophysiological hallmarks of the underlying inflammation driving psoriasis progression (*7, 8*), but cannot be accurately captured by PASI. Label-free imaging using UB-RSOM has recently afforded unique and highly detailed 3D images of the skin, resolving fine microvasculature and other skin morphological features that also serve as skin inflammation biomarkers (*9–14*).

To perform UB-RSOM, the region to be imaged is illuminated with low energy short light pulses (~1-10 ns). The light travels through tissue and a fraction of it is absorbed by chromophores, which in turn generate a tiny elevation of the local temperature (~0.001C^{o}). As a result, ultrasound waves (photoacoustic/optoacoustic waves) are produced. The ultrasound waves are detected by an ultra-broadband transducer and processed mathematically using tomographic principles to obtain the 3D distribution of light absorbers (more information on the arrangement of the illumination and transducer below). This light-in-sound-out scheme enables the detection of optical absorption at acoustic resolution in deep tissue, as image formation is governed by the diffraction of generated ultrasound waves and not by the diffusion of light, overcoming the low penetration depth of classical optical microscopy techniques (~0.2 mm). Thus, UB-RSOM, when using visible or near infrared light, produces 3D images of the most efficient light absorbers (haemoglobin and melanin) to resolve different skin features with up to sub-10 μm resolution, including capillary loops, the epidermis and, critically, dermal vasculature over several millimetres of depth. The method is well suited for longitudinal observations of human skin as it is non-invasive and does not require the use of contrast agents. UB-RSOM yields superior 3D and cross-sectional visualizations of microvasculature compared to other optical imaging methods, such as confocal microscopy, multi-photon microscopy (*15–17*), optical coherence tomography, or high-frequency ultrasonography

(*9*). With a detection bandwidth of more than 100 MHz, UB-RSOM offers the best combination of resolution and depth in dermatological imaging today (*18*) and enables novel means and contrast mechanism to investigate skin parameters, disease, and response to treatment.

To accurately identify skin features that are most responsive to treatment, we developed a second-generation UB-RSOM system (UB-RSOM 2G) that overcomes past technological limitations by integrating advanced motion correction and a novel skin placement design for repeatable data acquisition. We obtained 80 longitudinal UB-RSOM 2G scans from 20 psoriatic plaques under conventional treatment or receiving biologics treatment combined with topical corticosteroids (TCS) and reconstructed 3D skin images at 532 nm. Then, we employed image analytics to understand how treatment acts on different inflammation-associated microvasculature features and which of these features are most sensitive to disease remission. A second goal of the study was to explore imaging biomarkers that could capture healing patterns that are not apparent to the human eye or the PASI, better accommodating the demands of personalized precision medicine. We observe three, previously unknown, microvascular features that exhibit high sensitivity to treatment and could improve the precision by which skin and inflammatory changes are assessed.

RESULTS

UB-RSOM 2G device and its ability to image psoriatic skin

The UB-RSOM 2G device (Fig. 1, A to C) consists of a scan-head device that integrates a 2-fiber illumination unit and a broadband focused ultrasound detector mounted onto a set of mechanical stages (Fig. 1C) with 3 degrees of freedom (x,y,z). The x,y axes are used to raster scan the ultrasound detector and optical fiber bundle over the imaged skin region. For each point of the raster scan, a light pulse illuminates the tissue and the resulting optoacoustic wave-front is detected. The detected signals are filtered into two frequency bands for reconstruction: 10-42 MHz and 42-120 MHz. A low-frequency band image (rendered in red) and a high-frequency band image (rendered in green) are correspondingly reconstructed, frequency equalized (see Methods and (*9*)), and co-registered. Multi-color rendering and frequency equalization allow for the observation of fine spatial details together with lower-resolution skin structures that generally have greater intensities. The smallest capillaries appear in green and can be resolved from the melanin structures that appear in red. The larger microvessels in the horizontal plexus appear in yellow and red and can be easily distinguished from the green capillary loops (see Fig 1 and ref. (*9*)).

The z-axis allows the adjustment of the focal point of the transducer with respect to the skin surface. A control unit (Fig. 1B) integrates the laser source, alignment optics, data acquisition unit and electronics. Repeated measurements of identical sections of the dermal microvasculature over the course of treatment were enabled by the combination of UB-RSOM 2G's detachable interface unit and the use of ink fiducial markers (see fig. S1) and the 3 degrees of freedom of the mechanical stages.

Application of UB-RSOM 2G to healthy and psoriatic skin (Fig.1, D to G) allowed a side-by-side comparison of its performance in resolving relevant dermal features and confirm that UB-RSOM 2G produces detailed coronal (Fig. 1, D to E) and cross-sectional images (Fig. 1, F to G) of the skin. These images reveal the epidermis (EP) and the underlying dermal structures. In healthy skin, the melanin in the epidermis and the capillary loops (CL) in the dermal rete ridges,

which are interwoven with the epidermis, are clearly resolved. In the deeper dermal layer (DR), the subepidermal vascular plexus (SVP) and connecting vessels (CV) are visible. This general appearance changes in psoriatic skin, wherein UB-RSOM 2G captures the underlying acanthosis, the drastic elongation and dilation of the capillary loops, and an expansion of the sub-epidermal vascular plexus.

Histological analysis of regions scanned by UB-RSOM 2G corroborate the *in vivo* findings (Fig. 1, H to I). The histological slice of the healthy skin section (Fig. 1H) corresponding to the UB-RSOM 2G image in Fig. 1D,F shows the different layers of the epidermis and an ordered maturation of the keratinocytes. The thickness of the epidermis (123 μm) as measured from the subepidermal plexus to the skin surface by UB-RSOM 2G agrees with that observed in the histological slice (115 μm). The lengths of the capillary loops extending through the rete ridges are typical of healthy skin (*9*) (Fig. 2F, white arrows). Observation of the histological cross section of the psoriatic plaque (Fig. 1I) corresponding to the UB-RSOM 2G image in Fig. 1E,G shows hyperplastic epidermis pathology with aberrant replication of keratinocytes, as well as the elongation of the rete ridges. The elongated capillary loops "climb" through the rete ridges, a feature which is captured in vivo by UB-RSOM 2G (Fig. 1G, white arrows).

UB-RSOM 2G employs advanced motion correction algorithms to compensate for slight involuntary movements of the patients' body (Fig. 1, J to K and methods), which proved to be effective for psoriatic skin.

To assess in detail the ability of UB-RSOM 2G to quantify treatment efficacy, we longitudinally monitored 14 identical sections of 14 psoriatic plaques from 14 patients undergoing conventional inpatient treatment over the course of several days, as well as 6 psoriatic plaques from 5 patients during the initial phases of out-patient biological treatments over the course of several weeks. Conventional inpatient treatment included daily application of standard topical doses of salicylate vaseline, corticosteroids, dithranol, and simultaneous phototherapy (311 nm NB-UVB or PUVA). Patients in the biologics group, in addition to continuing their previously ineffective standard TCS therapy, received the IL17-inhibitor secukinumab (4 patients, subcutaneous injection) or the TNFα-inhibitor infliximab (1 patient, intravenous injection) according to the respective initiation scheme. For every patient, we analysed coronal images of the epidermis and cross-sectional images corresponding to the whole skin depth. The latter provided a comprehensive view of the microvascular structure while the former depicted the appearance of the capillary loops (Fig. 1, D to G).

UB-RSOM 2G biomarkers of psoriasis

A critical point herein was to examine the effect of treatment on different microvascular and other skin features that are uniquely resolved by UB-RSOM. We were interested to study whether different features respond differently to treatment, and which features were most sensitive to treatment and disease remission. The changing appearance of a representative plaque during the course of conventional treatment is displayed in Fig. 2. We obtained clinical and UB-RSOM 2G images before (day 1) and on days 5, 8 and 10 of the treatment (Fig. 2, A to L). We imaged the same location on the psoriatic plaque at every time point by making use of ink fiducial markers (see fig. S1). The clinical images (Fig. 2, A to D) show how the plaque improved from an initial severity visual score of PASI=7 to a score of PASI=2 at days 8 and 10, due to a major reduction

in redness and induration. The corresponding UB-RSOM 2G coronal views of the epidermis views show that the diameters of the capillary loops clearly decrease from the initial measurement to day 5, after which they appear to stabilize (Fig. 2, E to H). The UB-RSOM 2G cross section perspectives (Fig. 2, I to L) of the whole dermal depth reveal a more complete picture of how the treatment affects the microvascular structure of the psoriatic skin. Initially, the microvessels in the plexus appear densely packed and are barely resolved due to vasodilation and angiogenesis associated with the underlying inflammatory process (Fig. 2I). As a result, the subepidermal plexus appears both thick (as indicated by the mean plexus width, MPW in Fig. 2I) and dense. As treatment progresses, the microvascular stress supporting the inflammatory milieu decreases, with a subsequent reduction in the mean width of the subepidermal plexus (Fig. 2, J to L). Moreover, by day 8 the individual microvessels can be discerned due to a reduction in tortuosity and vasodilation (Fig. 2K). Importantly, the cross-sectional images also reveal how the lengths of the capillary loops decrease drastically.

This qualitative assessment of UB-RSOM 2G features was corroborated by image analysis to quantitatively study the relevance of particular skin features in relation to treatment progression. We extracted the mean capillary loop length (MCLL), mean capillary loop diameter (MCLD), and mean width (thickness) of the SVP (mean plexus width, MPW) because they correlated with the clinical response to treatment (improvement from PASI = 7 on day 1 to PASI = 2 on day 8, Fig. 2M). These three metrics relate directly to microvasculature, which is prominently affected by inflammation (*19*). The MPW decreased during the days of observation, from 0.46 mm to 0.29 mm (Fig. 2N). The MCLD, which corresponds to the mean width of the individual capillary loops measured in top view, decreased during the first 5 days of treatment, from an initial value of ~18 μm to stabilize between 13.5 μm and 14 μm (Fig. 2O). The MCLL exhibited consistent improvement with therapy over time, which manifested as an overall reduction in length from 0.55 mm to 0.27 mm (Fig. 2P), approaching the "healthy length" (~0.08 mm (*20*)).

In several cases, RSOM data recorded therapeutic effects over time that were not captured by the PASI. For example, one case demonstrated no change in PASI between days 8 and 10 (Fig. 2, A to L), whereas the MPW and MCLL showed clear evidence of skin recovery during the same time period (Fig. 2, N to P). We also observed cases where the PASI indicated that psoriatic skin was healed (Fig. 2, Q to R), whereas UB-RSOM 2G revealed residual pathological features of psoriasis (Fig. 2, S to T). These data were taken from a patient receiving biologics treatment. Despite the PASI indicating that complete healing was achieved at week 4 (Fig. 2U), UB-RSOM 2G imaging revealed a persisting but recovering pathological architecture of the microvasculature from week 4 to 5. In particular, UB-RSOM 2G recorded an MCLL decrease of 24% (from 264 μm to 200 μm) and an MPW decrease of 19% (from 367 μm to 298 μm; Fig. 2, V to W).

UB-RSOM 2G ability to monitor treatment

Observations of individual patients demonstrate the ability of UB-RSOM 2G to reveal highly detailed images of treatment and quantitatively compute image metrics that showcase higher sensitivity than PASI, however we also studied the ensemble of data to understand the trends in the entire collected dataset (Fig. 3). We plotted UB-RSOM 2G features, serving as treatment biomarkers, for all patients treated with conventional inpatient treatment (Fig. 3A, fig. S2a) or with biologics (Fig. 3B, fig. S2a) and extracted mean trends. The results were again contrasted with the current gold standard PASI both qualitatively and by calculating correlation values. Prior to treatment, the local PASI was similar in both groups, with a mean of 5.6 (range 4-8) in the

conventional treatment group and a mean of 5.0 (range 3-9) in the biologics treatment group (fig. S2a). After 6-13 weeks, the plaques treated with biologics healed better (mean PASI 0.6; 3 out of 6 reached PASI 0) than the plaques undergoing conventional treatment over the course of 9-10 days (mean PASI 2.2; 1 out of 14 reached PASI 0). The MCLL decreased monotonically in all patients (Fig. 3, A to B). During conventional treatment, the MCLL decreased on average from a value of 399 µm to 253 µm (-36.6%). The MPW also decreased monotonically for most patients and time points, declining by an average of 26.0% over the course of conventional treatment (Fig. 3A). Analogous trends in the MCLL and MPW were observed for the patients treated with biologics (Fig. 3B). The MCLD decreased with treatment in all skin sections, but its reduction was not as consistent as that of MCLL and MPW. Remarkably, the MCLL showed a great degree of correlation with PASI for both types of treatments (0.78, $P = 2\times10^{-5}$ for biologics and 0.74, $P = 2\times10^{-10}$ for conventional). The MPW showed a lower correlation with the PASI (0.52, $P = 0.01$ for biologics and 0.60, $P = 2\times10^{-6}$ for conventional), while the MCLP displayed the lowest correlation (0.48, $P = 0.03$ for biologics and 0.53, $P = 2\times10^{-4}$ for conventional; Fig. 3, C to E).

To offer an objective index that describes psoriasis remission and inflammatory burden, we compiled the quantified biomarkers into a psoriasis optoacoustic severity index (POSI, fig. S2b). The POSI combines the severity metrics of the MPW and the MCLL, i.e. the two biomarkers that were unambiguously affected by treatment. POSI mimics the local PASI, which could facilitate its clinical acceptance. More specifically POSI showed good correlation with the local PASI in this study (r^2=0.77, p=0.00004, fig. S2c), while also capturing subtle changes not reflected in the PASI scores.

In a pilot observational study, we compared the findings between patients treated with conventional therapy and patients treated with biologics. In particular, we compared the percentage change of the PASI with that of the UB-RSOM 2G biomarkers (fig. S3) in both patient groups. For patients undergoing conventional treatment, the MCLL, MPW, and MCLD decreased at similar rates during the initial phase of the treatment, while in patients treated with biologics there was a steeper decrease in the MCLL. This could indicate that during biologics treatment the length of the capillary loops – and possibly the strongly associated palpable and visible plaque induration – decrease faster, while other pathological features of the microvascular architecture that are invisible to superficial clinical assessment may persist. An observation of this effect has not been possible until now. Although the clinical implications remain unclear and the analysis was based only on a small number of patients, this result demonstrates the potential of UB-RSOM 2G to yield deeper insights into the physiology of both the disease and its treatment.

Repeatability study

The variable pressure exerted by the scan-head on the skin might compress the dermis and corrupt biomarker calculations. To confirm the quality of the data and that the fine differences captured by RSOM 2G were not the result of noise, motion, or errors introduced by the device operator during data collection, we conducted a repeatability study. Data was acquired from 9 plaques at two time points, 10 minutes apart, after removing and repositioning the RSOM scan-head between scans, guided by the ink fiducial markers. UB-RSOM 2G biomarkers were computed for all images and a repeatability coefficient was calculated using an ANOVA model (*21*), which represents the absolute difference between two repeated results with a probability of 95%. The differences in the $t = 0$ min and $t = 10$ min time-points revealed that repeating the scan-head placement affords only small discrepancies in positioning of a few hundred micrometers (Fig. 4,

A to B). As a result, in. some cases, we observed that the images captured at the two time points were shifted relative to each other; however, matching anatomical features could be easily recognized in both images. The computation of UB-RSOM 2G biomarkers showed little difference in values between T=0 and T=10 min. For example, the MCLL and MPW values showed a repeatability coefficient of 36.7 μm and 38.4 μm, respectively (Fig. 4, C to E).

For the three computed biomarkers (MCLL, MPW, MCLD), the quantification accuracy is given by the axial resolution of the system. The RSOM system employed herein has a resolution of ~7 μm through the whole dermis (*9*) which implies that both repeatability analysis and the overall trends observed in Fig. 2 and Fig. 3 are not affected by the system's resolution. The repeatability study also showed that the biomarker changes computed as a function of treatment were not a result of system or operator errors (e.g. the effect of variable pressure on skin) but instead represent true microvasculature changes due to the treatment and disease remission. For example, in the case corresponding to the difference between day 8 and day 10 shown in Fig.2, the MPW decreased by 56 μm and the MCLL decreased by 49 μm while PASI remained constant (Fig.2, M,O,P), while the repeatability coefficients are 38.4 and 36.7 respectively.

Correlation between the RSOM biomarkers and DQLI

Quantitative markers of treatment as afforded by the UB-RSOM 2G biomarkers are useful for assessing response to treatment, however it is important to also consider more subjective indications of treatment efficacy, such as patient-reported symptoms. We therefore gathered response-to-treatment dermatology life quality index (DLQI) data for 83% of the biologic therapy patients (fig. S5). We found a positive correlation for both the MCLL (pearson correlation coefficient 0.72, p=0.008) and the MPW (pearson correlation coefficient 0.78, p=0.003). DLQI was not available for the patients that received conventional therapy.

DISCUSSION

In this study, we monitored the treatment of psoriasis using computed biomarkers extracted from detailed, 3D images including epidermis and dermis generated by a second-generation UB-RSOM device with advanced placement and motion correction technology. This approach is markedly different from the current method of psoriasis assessment, which only evaluates response based on subjective visual and palpatory examinations of lesions by physicians. By providing a complete picture of the disease, including sub-surface features at resolutions of 10 μm or better, UB-RSOM 2G affords more detailed observations of inflammatory features based on microvasculature and other morphological biomarkers. Furthermore, this study yielded unprecedented insights into the effects of conventional and biologics treatments on psoriatic lesions. We found that treatments led to large changes in the length of the capillary loops and the width of the subepidermal plexus. Such changes continue even when clinical evaluation (PASI) indicates that a plaque is unchanging. Elongation of the capillary loops is a well-known marker of psoriatic skin in histological assessment (*1*). However, until now this parameter could not be directly and non-invasively quantified *in vivo*.

We found the MCLL and MPW to be the most sensitive parameters to treatment. These biomarkers could be used to construct the POSI, which could offer a more precise index than PASI for treatment and disease characterization. MCLL and MPW elucidated changes in skin

microvasculature that were more subtle than those revealed by the more subjective PASI grading. The MCLL and MPW thus allowed us to observe and quantify improvements in psoriatic skin where no visible change was apparent or recorded by the PASI, which reflects the high accuracy and precision of RSOM. A quantitative comparison between the accuracy and precision of the RSOM biomarkers and the PASI components is not a straightforward task because of the subjective nature of the latter. However, some conclusions can be derived. For example, it is generally accepted that the accuracy of the induration component of the PASI (thickness of the plaque) is 250 µm, which corresponds to the resolution of the average human eye. This implies that the RSOM biomarkers improve upon the accuracy of the PASI component by 2 orders of magnitude (the axial resolution of UB-RSOM 2G is ~7 µm). On the other hand, the concepts of "redness" and "degree of scaling" included in the PASI are difficult to put into context against the micrometer resolution biomarkers obtained by RSOM. Overall, the objective nature of optoacoustic biomarkers (precision) and their low error due the method's high resolution (accuracy) leads to better sensitivity. Higher sensitivity here means that UB-RSOM 2G is able to show healing effects that were not previously detectable by clinical assessment and reveal subtle pathology when the PASI indicates healthy skin. For the sake of completeness we have to point out that we also found that the measurements of MCLD were slightly affected by blurring due to unknown sources of error, which may include wrong reconstruction parameters estimation.

The ability to observe fine skin parameters associated with inflammatory burden could both improve and personalize treatment monitoring and drug development. The quantification of changes in representative portions of the skin during treatment with high sensitivity to therapy could lead to more accurate assessments of treatment efficiency, serving the goals of precision medicine by offering objective biomarkers that are urgently needed (*22*). UB-RSOM 2G could aid in selecting the most suitable therapy for an individual and in the precise monitoring of the patient's early response to treatment. Considering the high long-term costs of psoriasis therapy, particularly when using biologics, individualized therapies (e.g., tailored application frequencies) would benefit both the patient and the healthcare system. New metrics are also needed for drug development, because PASI lacks responsiveness and sensitivity in the case of mild disease (*6*). New biologics for psoriasis treatment are being developed and continue to enter the market. Due to their overall high efficacies, it is increasingly important to be able to observe slight differences in treatment response not allowed by PASI. UB-RSOM 2G could therefore be useful for drug discovery or clinical decision making about treatment selection and drug dosing. By revealing pathological states of skin not detectable by the current standard, the use of optoacoustic biomarkers could improve decisions regarding treatment termination and areas of application, the latter for the specific case of topical conventional treatment.

UB-RSOM 2G offers compelling advantages for treatment assessment over other imaging methods in dermatology. Optical microscopy methods, such as reflectance confocal microscopy (RCM) and multiphoton microscopy (MM), can image superficial pathological features of psoriatic skin, such as parakeratosis, spongiosis, inflammatory cells and the dilation of the capillary loops[5-7]. However, the typical penetration depths of ~100 µm for RCM and MM are insufficient to visualize the subepidermal vascular plexus or precisely measure the full lengths of microvessels from their origins in the plexus. Even psoriatic plaques with "moderate" induration according to PASI grading can reach thicknesses of 0.5 mm or more. Optical coherence tomography (OCT) and high frequency ultrasound (HFUS) can offer deeper imaging. Pilot OCT

studies found that the epidermal thickness (ET) may decrease during psoriasis therapy, but although the changes were statistically significant they were small in magnitude and do not allow for a direct assessment of the underlying inflammation (*23–28*). Although OCT-based angiography can visualize superficial microvessels, the method is inappropriate to comprehensively assess the capillary loops and image the subepidermal vascular plexus in thickened psoriatic skin, since it cannot produce high-quality 3D images of the skin due to strong inherent artefacts in the axial direction (*29–31*). Moreover, the optoacoustic contrast from microvessels, which stems from the strong optical absorption of haemoglobin, is superior to that of OCT, which indirectly detects blood via flow-related signals. The contrast of microvessels is even poorer in HFUS. Label-free HFUS only detects vessels larger than 100 µm (*32*), which is far above the diameter of most dermal microvessels. Photography-based machine learning algorithms have recently been introduced, which are capable of determining local PASI and the affected body surface (*33*). While these methods can be more objective and reliable than conventional PASI assessments, their dependence on superficial information fundamentally limits these methods to the same features evaluated by PASI. Integrating such methods with RSOM could eventually afford a most powerful approach for the determination of psoriasis severity.

With the recent evolution of laser-diode sources with the potential to reach sufficiently high energy levels for RSOM (*34*), the UB-RSOM system is expected to have a cost of components in the few thousand of euro, with mass production further reducing this cost. At such cost of materials, the technology offers a viable solution for dermatology clinics and high dissemination potential. Nevertheless, several improvements to the UB-RSOM 2G system are being made based on feedback from clinical users to overcome practical constraints that may hinder the wide adoption of the technology. One such future development is the construction of an enclosed interface unit with automatic water filling to avoid leakage and enable imaging at tilt angles that are higher than the 30º angle that is currently possible. Another future development is directed toward adding an optical camera detector that can use pattern recognition methodology, based on anatomical references, to avoid the necessity of fiduciary for ensuring repeatable placement on the same skin location over longitudinal measurements. Such improvements can also reduce the procedure time that it takes to obtain a scan. Currently, a trained user can place the system and obtain an image in 7-10 min. Next generation systems will aim to be able to place the system on the skin and obtain the required image in about 1 minute.

Clinical acceptance of a novel modality is a complex process that depends on a multiple parameters, including cost, overall benefit, ease of use, health risk, and overall performance related to the state-of-the-art. UB-RSOM 2G is a strong candidate for future routine use in dermatology because it is a noninvasive optical technique with unique imaging capabilities. UB-RSOM 2G could provide objective precision measurements of subsurface skin features that augment scores of a patient's subjective symptoms and quality of life to improve clinical decision making. Preliminary, we showed that the response to therapy seen by the RSOM biomarkers correlated with the DLQI for a subset of patients, however future studies should focus on correlating objective readings with subjective symptoms. Our results indicate that UB-RSOM 2G is well suited to observe and quantify treatment success in representative psoriasis plaques. Further work will elucidate if measuring a greater number of plaques in different parts of the body will prove more beneficial for quantifying the overall treatment success.

In this second-generation system, we have already incorporated methods for improved placement and motion correction to offer accurate measurements in a portable, handheld format. Further work should optimize the water handling and the acquisition time for a better compatibility of the system in the clinical routine. The repeatability study showcased that, although the resolution of the system is ~7 μm the precision of the system was ~36-38 μm due to motion and placement errors. We anticipate that this pilot study will trigger a larger range of independent investigations into novel psoriasis pharmaceuticals. It is critical that such future studies quantify reproducibility in a manner similar to the present work to clearly identify the accuracy of the method at different operator experiences. It is important to compute the inter-operator error to identify whether new designs for placement and motion correction are required to further improve the precision towards the theoretical limit (<10 μm).

MATERIALS AND METHODS

Study design

Response to treatment

The protocol for the therapy response study was approved by the Ethics Committee of the Faculty of Medicine of the Technical University of Munich. A total of 19 patients participated in the study (14 men, 5 women, age 22-68, mean age 44.1) after giving written informed consent. All participants were patients of the Department of Dermatology at the university hospital of the Technical University of Munich and had been diagnosed with plaque psoriasis, which was confirmed by histology. The study included one group (group A) of patients undergoing conventional and one group (group B) of patients being treated with biologics in addition to continuing their previously ineffective therapies with topical corticosteroids (TCS). 14 patients were monitored during conventional inpatient treatment consisting of topical descaling, anti-inflammatory therapy (by means of salicylate vaseline, topical corticosteroids and dithranol) and simultaneous phototherapy (311 nm Narrowband UVB (NB-UVB) or psoralen-UVA (PUVA)). The first measurement was performed using the UB-RSOM 2G immediately prior to therapy and measurements were taken on day 1 (14 plaques), day 3 (12 plaques), once between day 4 to 6 (9 plaques), once between day 7 to 8 (9 plaques) and once between days 9 to 10 (9 plaques). The fact that not all patients could be measured at all time points was due to limits on the durations of their stays in the hospital and lack of patient access on weekends. A procedure using ink fiducial markers was established to image the same section of the psoriasis plaques over time (fig. S1). The 5 patients included in group B were imaged before and during therapy with the biologics infliximab (1 patient) and secukinumab (4 patients) and standard TCS therapy. In one of these patients, two plaques were monitored, resulting in 6 plaques examined in group B. Measurements were taken prior to therapy at week 1 (6 plaques), week 2 (2 plaques), week 3 (3 plaques), week 4 (3 plaques), week 5 (4 plaques) and once between week 6 and 13 (5 plaques). By using photos and anatomical landmarks, the imaged part of the monitored psoriasis plaques was kept as similar as possible between the measurements. Histology was taken once from the monitored plaque in one patient before undergoing conventional treatment.

Repeatability

The therapy response study protocol was approved by the Ethics Committee of the Faculty of Medicine of Technical University of Munich. A total of 9 patients participated in the study (4 men, 5 women, age 19-51, mean age 32.1) after giving written informed consent. All participants were patients of the Department of Dermatology at the university hospital of the Technical University of Munich and had been diagnosed with plaque psoriasis, which had been confirmed by histology. The repeatability study was designed following the guidelines that can be found in (*21*). For each patient, two measurements of the same plaque were recorded 10 min apart using the UB-RSOM 2G. After the first measurement, the scan head was completely removed from the patient and replaced after the ten minutes. Between measurements the patient was free to move or walk. The ink fiducial marker procedure was used for placements of the scan head. The MCLL, MPW and MCLD parameters were derived for each measurement using the same procedure as described below for the conventional psoriasis therapy monitoring study.

UB-RSOM 2G system, motion correction and image reconstruction

The UB-RSOM 2G system was built in-house. For light excitation, the system uses a 532 nm Nd:YaG laser (Wedge HB.532, Bright-solutions SRL) at a pulse length of 0.9 ns to induce the broadband optoacoustic signals. Experiments were conducted using a 500 Hz repetition rate, at which the light energy delivered to the skin surface does not exceed 3.75 μJ/mm^2, thereby complying with the safety limits of laser exposure specified by the American National Standards Institute. The UB-RSOM 2G system scan head includes a spherically focused piezoelectric transducer (frequency range 10-120 MHz) with a central frequency of 55 MHz (Sonaxis). The transducer is attached to three motorized stages: the x,y stages (size, 35 mm × 35 mm × 15 mm; Physik Instrumente) and the z stage (MTS50-Z8, ThorlabsThe x-y stages are used to scan the transducer and fibre bundles along a grid that yields a 4 x 2 mm field-of-view. The acquisition step is 20 μm and the acquisition time is 70 s (8.75 s/mm^2).
The scan head also integrates the illumination bundles. An interchangeable interface unit shielded with an optically and acoustically transparent plastic membrane is placed below the scan-head. The interface unit is filled with 1.5 ml of water and enables the acoustic coupling between the skin and the transducer detection surface. Once the unit is filled, the system is easily placed onto the desired skin area.
Prior to scanning, the z-axis motorized stage is used to place the transducer at the desired height above the skin surface (the focal point should be ~100 to 300 μm above the skin). After acquisition, the detected signals are filtered using a 4th order butterworth filter into two frequency bands for reconstruction: 10–42 MHz and 42–120 MHz. A low-frequency band image and a high-frequency band image are correspondingly reconstructed by applying the so-called universal back projection algorithm (*35*) to account for the out-of-focus signals. For representation an RGB image is constructed in which the low frequency band reconstruction occupies the red channel and the high frequency reconstruction the green channel. The high frequency reconstruction is multiplied by a parameter which is calculated by solving the optimization problem described in (*9*). Such an equalization operation increases the intensity of the high frequencies, partially taking into account the effects of the acoustic absorption in tissue, enabling size-dependent discrimination of tissue structures (see Methods and (*9*)) as well as their co-registration. Further technical details of the

system have been described in (*9*). Major improvements in comparison to previous versions of UB-RSOM include: the use of a motorized z-stage for precise adjustment of the ultrasound transducer's focal point slightly above the skin surface and the implementation of a novel motion correction algorithm (*36*) that improves the sensitivity of the reconstruction image to motion over previously published methods, and that was applied for psoriasis imaging for the first time. In such studies the success of the motion correction algorithm relied on the presence of artefacts in the acquired data generated by the epidermal melanin layer. However, there is a drastic reduction in melanin in psoriatic skin, reducing the effectiveness of the algorithm. The system also includes an integrated miniature preamplifier (30 dB amplification, ERA-8SM+, Mini-Circuits) on the ultrasound transducer to amplify the signal before transmission to the acquisition card, which improves the overall signal to noise ratio of the images. Additionally, the use of cylindrical bundles that are raster-scanned together with the transducer instead of fixed rectangular bundles leads to more efficient illumination and better signal to noise ratio. The use of an articulated arm with 3 degrees of freedoms (rotulas) and a single screw to simultaneously tighten (DG Holder, NOGA) all the rotulas improves the usability of the system.
The resolution of the system is ~30 µm (lateral) and ~7 µm (axial) up to ~ 1.2 mm deep. From 1.2 mm to 2.5 mm the resolution worsens to 10 µm. Further degradation is expected beyond those depths due to the attenuation of the high-frequency components of the ultrasound signal by tissue. A detailed assessment on the resolution of the system can be found in (*9*).

Imaging identical sections of psoriasis plaques during conventional therapy

To image identical sections of the monitored psoriasis plaques in those patients undergoing conventional therapy, the area of interest was marked using two green ink dots (fig. S1). The dots were separated by a 4 mm gap, which corresponded to the width of the chosen transverse field-of-view. Before each imaging session, the scan head was first manually positioned using UB-RSOM 2G's detachable interface unit such that the ink dots macroscopically marked the limits of the field-of-view. Consequently, the ink dots' optoacoustic signals were identified using short pre-acquisitions. Then, the home position of the transducer was adjusted to maintain the field-of-view precisely between the dots, with them centred on the sagittal axis.

Quantification of disease hallmarks and correlation with PASI

Once images were acquired and reconstructed, the first step to obtain features resolved by UB-RSOM 2G was to flatten the skin surface in the reconstructed images. This step was performed manually as follows: the whole 3D image was divided into 20 µm thick slices in the y-direction (Fig. 1F). For each slice, the maximum intensity projection (MIP) along the y-direction was calculated. In the MIPs, the skin surface can be observed univocally. For every MIP, the operator placed ten points along the surface of the skin. Using an interpolation algorithm based on spline functions, whole surfaces were extracted and the skin was flattened (fig. S4). The maximum intensity projection image along the y-axis was subsequently computed from the flattened skin images.

The mean capillary loop length (MCLL), mean capillary loop diameter (MCLD), mean width (thickness) of the subepidermal vascular plexus (mean plexus width, MPW) were calculated

manually from the MIP (fig. S4). The total blood volume, fractal number of the vascular structures and the ratio of low-to-high frequency content of the optoacoustic signal were calculated as explained in (*9*).

Statistical analysis

The repeatability coefficient was calculated as $1.96 \times \sqrt{2} \times std$ were std is the within subject standard deviation and was calculated using a one way analysis of variance (ANOVA) using Matlab, assuming normality in the error distribution. Normality was checked using the Anderson-Darling test. Data for the repeatability test is available in the supplementary material as an excel file.

Acknowledgments: The authors would like to thank Robert J. Wilson for editing the manuscript.

Funding:

This project was funded by the German Society of Dermatology (DDG, German Psoriasis Price to JA), the European Commission ("INNODERM" no. 687866 and "WINTHER" no. 871763 to VN) and the German Research Foundation (DFG, 435874434/A2) to TB.

Author contributions:

Conceptualization: JA, VN, BH
Methodology: JA, BH
Data curation: BH, JA, TN, AB, LE
Investigation: JA, BH
Visualization: JA, AB
Funding acquisition: JA, VN, TB
Project administration: JA, VN, UD, TB
Supervision: JA, VN, UD, TB, KE, FL
Writing – original draft: JA, BH, VN

Competing interests:

J.A. is co-inventor of the patent applications EP2946721A1 and EP3654828A1 held by the Helmholtz Zentrum München that covers aspects of Raster Scan Optoacoustic Mesoscopy. V.N. has financial interests in iThera Medical GmbH.

Data and materials availability: All data associated with this study are present in the paper or the Supplementary Materials. Reasonable requests will be granted with permission of the Klinik und Poliklinik für Dermatologie und Allergologie am Biederstein, Munich, Germany. Figures in blue and green colormaps are available for the colorblind reader.

Supplementary Materials:

Materials and Methods

Fig. S1 to S5

Data file S1

MDAR Reproducibility Checklist

References

1. F. O. Nestle, D. H. Kaplan, J. Barker, Psoriasis. *The New England journal of medicine*. **361**, 496–509 (2009).
2. W.-H. Boehncke, M. P. Schön, Psoriasis. *The Lancet*. **386**, 983–994 (2015).
3. T. Wong, L. Hsu, W. Liao, Phototherapy in psoriasis: a review of mechanisms of action. *Journal of cutaneous medicine and surgery*. **17**, 6–12 (2013).
4. R. B. Warren, M. Gooderham, R. Burge, B. Zhu, D. Amato, K. H. Liu, D. Shrom, J. Guo, A. Brnabic, A. Blauvelt, Comparison of cumulative clinical benefits of biologics for the treatment of psoriasis over 16 weeks: Results from a network meta-analysis. *Journal of the American Academy of Dermatology*. **82**, 1138–1149 (2020).
5. *PASImeter Psoriasis severity index: Photographic guide,* https://www.dermatools.net/dam/jcr:f95c96d7-cec5-4a25-ab3b-a1e3b2b4d5e0/PASIMETER-Photographic-Pr%C3%A4sentationmdus.pdf.
6. P. I. Spuls, L. L. A. Lecluse, M.-L. N. F. Poulsen, J. D. Bos, R. S. Stern, T. Nijsten, How good are clinical severity and outcome measures for psoriasis?: quantitative evaluation in a systematic review. *The Journal of investigative dermatology*. **130**, 933–943 (2010).
7. C. E. M. Griffiths, J. N. Barker, Pathogenesis and clinical features of psoriasis. *The Lancet*. **370**, 263–271 (2007).
8. C. Ryan, N. J. Korman, J. M. Gelfand, H. W. Lim, C. A. Elmets, S. R. Feldman, A. B. Gottlieb, J. Y. M. Koo, M. Lebwohl, C. L. Leonardi, A. S. van Voorhees, R. Bhushan, A. Menter, Research gaps in psoriasis: opportunities for future studies. *Journal of the American Academy of Dermatology*. **70**, 146–167 (2014).
9. J. Aguirre, M. Schwarz, N. Garzorz, M. Omar, A. Buehler, K. Eyerich, V. Ntziachristos, Precision assessment of label-free psoriasis biomarkers with ultra-broadband optoacoustic mesoscopy. *Nat Biomed Eng*. **1**, 496 (2017).
10. B. Hindelang, J. Aguirre, M. Schwarz, A. Berezhnoi, K. Eyerich, V. Ntziachristos, T. Biedermann, U. Darsow, Non-invasive imaging in dermatology and the unique potential of raster-scan optoacoustic mesoscopy. *Journal of the European Academy of Dermatology and Venereology : JEADV* (2018).
11. A. Berezhnoi, J. Aguirre, B. Hindelang, N. Garzorz-Stark, M. Omar, U. Darsow, K. Eyerich, V. Ntziachristos, Optical features of human skin revealed by optoacoustic mesoscopy in the visible and short-wave infrared regions. *Opt. Lett.* **44**, 4119–4122 (2019).
12. J. Aguirre, B. Hindelang, A. Berezhnoi, U. Darsow, F. Lauffer, K. Eyerich, T. Biedermann, V. Ntziachristos, Assessing nailfold microvascular structure with ultra-wideband raster-scan optoacoustic mesoscopy. *Photoacoustics*. **10**, 31–37 (2018).

13. B. Hindelang, J. Aguirre, A. Berezhnoi, T. Biedermann, U. Darsow, B. Eberlein, V. Ntziachristos, Quantification of skin sensitivity to ultraviolet radiation using ultrawideband optoacoustic mesoscopy. *The British journal of dermatology*. **184**, 352–354 (2021).
14. B. Hindelang, J. Aguirre, A. Berezhnoi, H. He, K. Eyerich, V. Ntziachristos, T. Biedermann, U. Darsow, Optoacoustic mesoscopy shows potential to increase accuracy of allergy patch testing. *Contact Dermatitis*. **83**, 206–214 (2020).
15. F. Lacarrubba, G. Pellacani, S. Gurgone, A. E. Verzì, G. Micali, Advances in non-invasive techniques as aids to the diagnosis and monitoring of therapeutic response in plaque psoriasis. *International journal of dermatology*. **54**, 626–634 (2015).
16. M. Agozzino, C. Noal, F. Lacarrubba, M. Ardigò, Monitoring treatment response in psoriasis. *Psoriasis (Auckland, N.Z.)*. **7**, 27–34 (2017).
17. M. Ardigò, M. Agozzino, C. Longo, A. Lallas, V. Di Lernia, A. Fabiano, A. Conti, I. Sperduti, G. Argenziano, E. Berardesca, G. Pellacani, Reflectance confocal microscopy for plaque psoriasis therapeutic follow-up during an anti-TNF-α monoclonal antibody. *Journal of the European Academy of Dermatology and Venereology : JEADV*. **29**, 2363–2368 (2015).
18. M. Omar, J. Aguirre, V. Ntziachristos, Optoacoustic mesoscopy for biomedicine. *Nat Biomed Eng*. **3**, 354–370 (2019).
19. S. C. A. Hanssen, C. J. M. van der Vleuten, P. E. J. van Erp, M. M. B. Seyger, P. C. M. van de Kerkhof, The effect of adalimumab on the vasculature in psoriatic skin lesions. *The Journal of dermatological treatment*. **30**, 221–226 (2019).
20. I. M. Braverman, A. Yen, Ultrastructure of the human dermal microcirculation. II. The capillary loops of the dermal papillae. *The Journal of investigative dermatology*. **68**, 44–52 (1977).
21. J. W. Bartlett, C. Frost, Reliability, repeatability and reproducibility: analysis of measurement errors in continuous variables. *Ultrasound in obstetrics & gynecology : the official journal of the International Society of Ultrasound in Obstetrics and Gynecology*. **31**, 466–475 (2008).
22. N. J. Schork, Personalized medicine. *Nature*. **520**, 609–611 (2015).
23. H. Morsy, S. Kamp, L. Thrane, N. Behrendt, B. Saunder, H. Zayan, E. A. Elmagid, G. B. E. Jemec, Optical coherence tomography imaging of psoriasis vulgaris. *Archives of dermatological research*. **302**, 105–111 (2010).
24. J. Welzel, M. Bruhns, H. H. Wolff, Optical coherence tomography in contact dermatitis and psoriasis. *Archives of dermatological research*. **295**, 50–55 (2003).
25. K. Buder, P. Knuschke, G. Wozel, Evaluation of methylprednisolone aceponate, tacrolimus and combination thereof in the psoriasis plaque test using sum score, 20-MHz-ultrasonography and optical coherence tomography. *International journal of clinical pharmacology and therapeutics*. **48**, 814–820 (2010).
26. J. Olsen, J. Holmes, G. B. Jemec, Advances in optical coherence tomography in dermatology-a review. *Journal of biomedical optics*. **23**, 1–10 (2018).
27. M. L. Musumeci, F. Lacarrubba, C. M. Fusto, G. Micali, Combined clinical, capillaroscopic and ultrasound evaluation during treatment of plaque psoriasis with oral cyclosporine. *International journal of immunopathology and pharmacology*. **26**, 1027–1033 (2013).

28. F. Lacarrubba, B. Nardone, M. L. Musumeci, G. Micali, Ultrasound evaluation of clobetasol propionate 0.05% foam application in psoriatic and healthy skin: a pilot study. *Dermatologic therapy*. **22 Suppl 1**, S19-21 (2009).
29. G. Odorici, A. Losi, S. Ciardo, G. Pellacani, A. Conti, Non-invasive evaluation of Secukinumab efficacy in severe plaque psoriasis with confocal microscopy and optical coherence tomography. *Skin research and technology : official journal of International Society for Bioengineering and the Skin (ISBS) [and] International Society for Digital Imaging of Skin (ISDIS) [and] International Society for Skin Imaging (ISSI)*. **24**, 160–162 (2018).
30. A. J. Deegan, F. Talebi-Liasi, S. Song, Y. Li, J. Xu, S. Men, M. M. Shinohara, M. E. Flowers, S. J. Lee, R. K. Wang, Optical coherence tomography angiography of normal skin and inflammatory dermatologic conditions. *Lasers in surgery and medicine*. **50**, 183–193 (2018).
31. S. Schuh, J. Holmes, M. Ulrich, L. Themstrup, G. B. E. Jemec, N. de Carvalho, G. Pellacani, J. Welzel, Imaging Blood Vessel Morphology in Skin: Dynamic Optical Coherence Tomography as a Novel Potential Diagnostic Tool in Dermatology. *Dermatology and therapy*. **7**, 187–202 (2017).
32. C. Errico, J. Pierre, S. Pezet, Y. Desailly, Z. Lenkei, O. Couture, M. Tanter, Ultrafast ultrasound localization microscopy for deep super-resolution vascular imaging. *Nature*. **527**, 499–502 (2015).
33. C. Fink, C. Alt, L. Uhlmann, C. Klose, A. Enk, H. A. Haenssle, Precision and reproducibility of automated computer-guided Psoriasis Area and Severity Index measurements in comparison with trained physicians. *The British journal of dermatology*. **180**, 390–396 (2019).
34. A. Stylogiannis, L. Prade, A. Buehler, J. Aguirre, G. Sergiadis, V. Ntziachristos, Continuous wave laser diodes enable fast optoacoustic imaging. *Photoacoustics*. **9**, 31–38 (2018).
35. M. Xu, L. V. Wang, Universal back-projection algorithm for photoacoustic computed tomography. *Physical review. E, Statistical, nonlinear, and soft matter physics*. **71**, 16706 (2005).
36. J. Aguirre, A. Berezhnoi, H. He, M. Schwarz, B. Hindelang, M. Omar, V. Ntziachristos, Motion Quantification and Automated Correction in Clinical RSOM. *IEEE transactions on medical imaging*. **38**, 1340–1346 (2019).

Figures

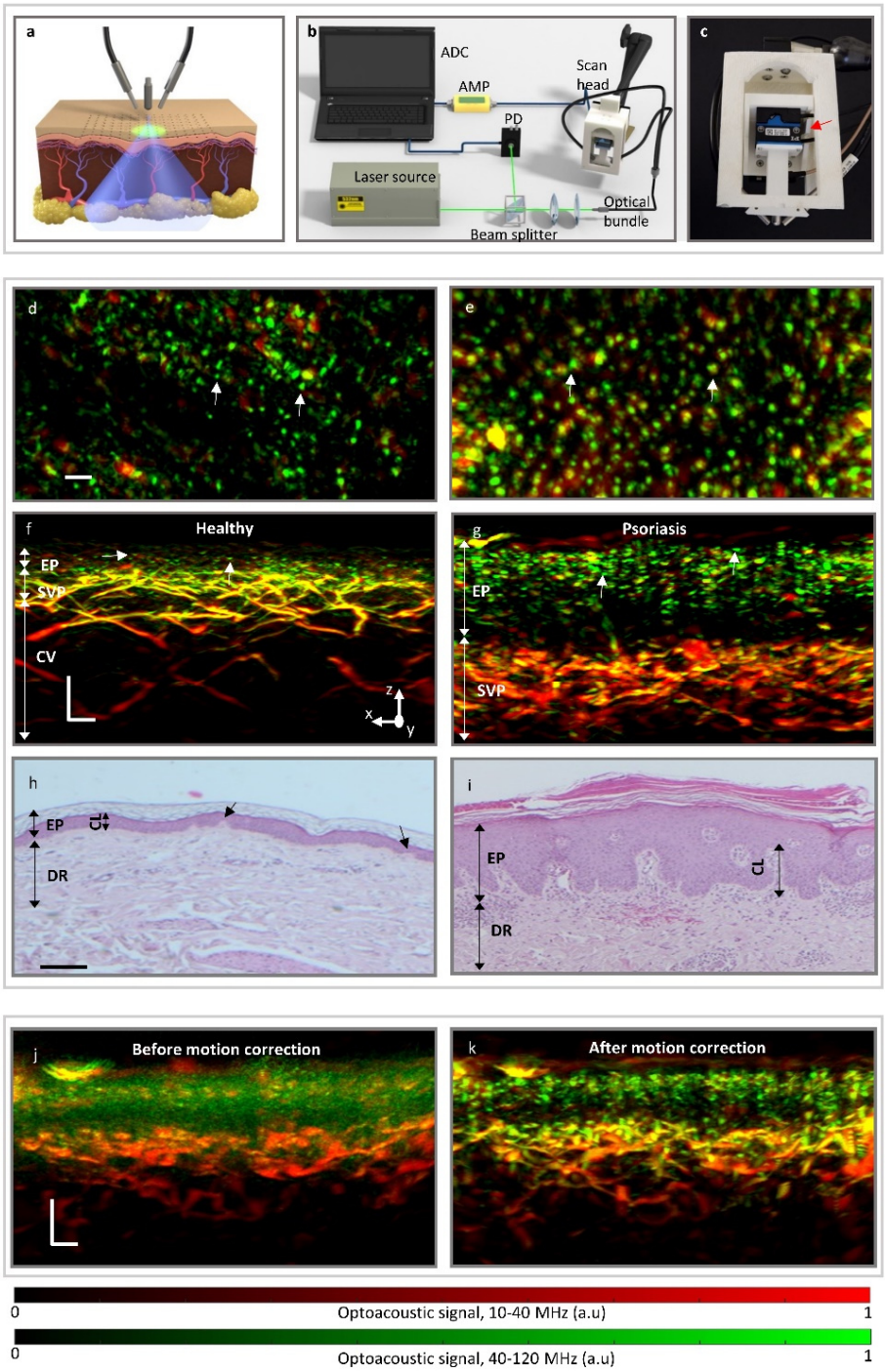

Fig. 1. Precision imaging of psoriasis using UB-RSOM 2G. (A) UB-RSOM 2G in use showing optical fiber bundles for illumination and a transducer that is raster-scanned parallel to the skin surface. **(B)** UB-RSOM 2G system. A laser pulse is directed to the sample. A part is diverged to a photodiode (PD), triggering the analog-to-digital convertor (ADC). The optoacoustic signals are amplified (AMP) and sent to the ADC. The transducer is in the scanning head. An interface unit

ensures proper attachment to the skin. **(C)** Photograph of the scanning head with three stages, each of them a spatial axis (red arrow). **(D)** UB-RSOM 2G coronal section of healthy epidermis (EP), and dermal rete ridges containing capillary loops (CL; green dots, white arrows). **(E)** UB-RSOM 2G coronal section of the epidermis and dermal rete ridges of psoriatic skin. **(F)** UB-RSOM 2G cross-sectional image of healthy human skin showing the EP and vessels in the dermis consisting of the subepidermal vascular plexus (SVP) and the connecting vessels (CV). CL tips are visible (white arrows). Double-headed arrows indicate the layers containing the EP, SVP, and CV. **(G)** UB-RSOM 2G cross-sectional image of psoriatic skin. CL (white arrows) appear in green, interleaved with widened epidermal structures (EP, red). A dilated and dense widened SVP is also present. Double-headed arrows indicate the layers containing the EP and SVP. **(H)** Histological cross-section of the same area depicted in (D, F). Small rete ridges can be observed, which contain the CL (black arrows). **(I)** Histological cross-section of the same area as depicted in (E, G) showing acanthosis, hyperkeratosis, and and elongated CL. The SVP in the upper dermis (DR) appears dilated. **(J-K)** UB-RSOM 2G image of psoriasis before and after motion correction. Scale bars 200 μm.

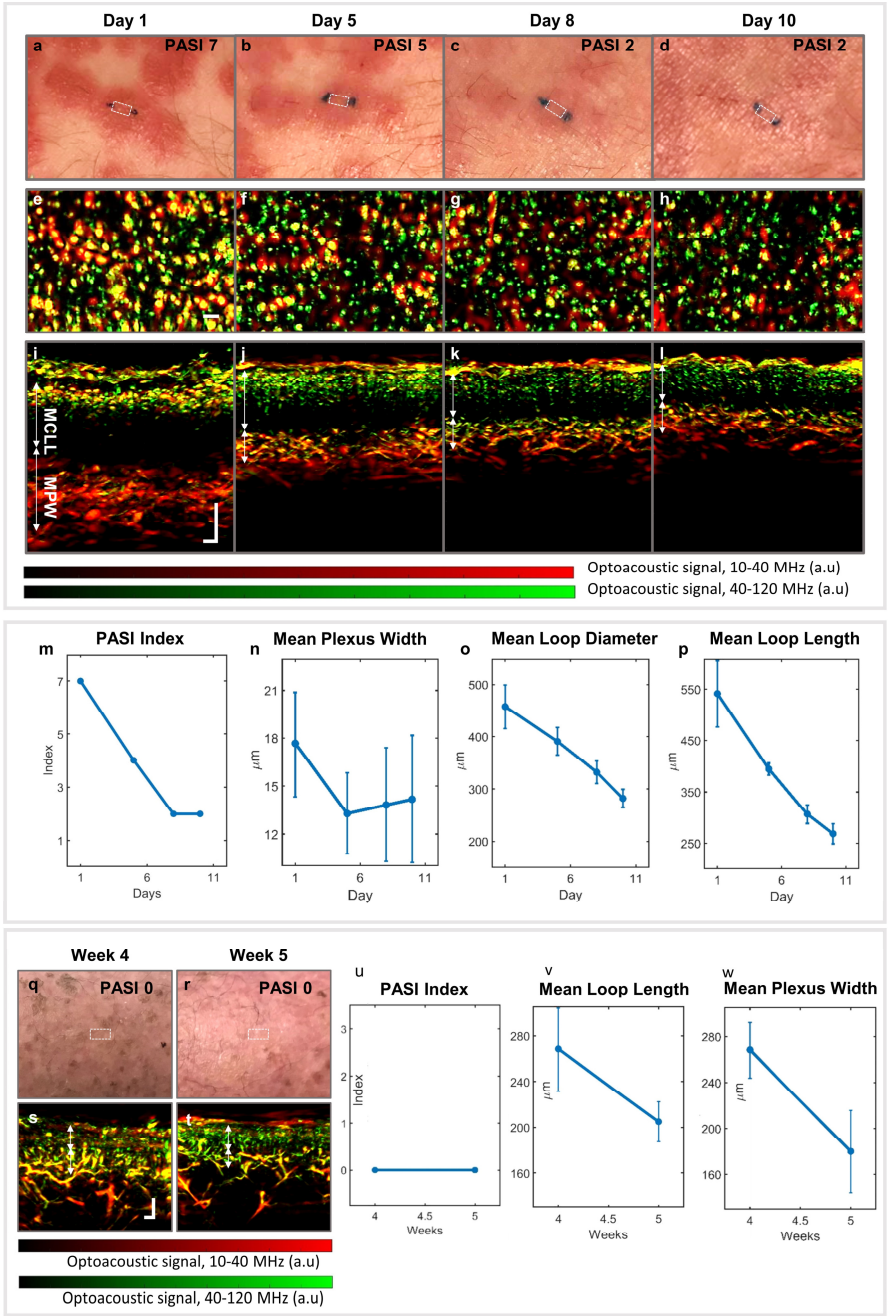

Fig. 2. Clinical views of psoriatic plaque during conventional therapy, and the corresponding coronal and cross-sectional UB-RSOM 2G images. (A to D) Clinical photographs of the same psoriatic plaque on days 1, 5, 8, and 10 of conventional treatment with the PASI value indicated in the top right. Ink fiducial markers (two dark green dots) ensure that the imaged section of the dermal vasculature is reproduced (see fig. S1). **(E to H)** Coronal UB-RSOM 2G images corresponding to the white dotted rectangles in the clinical photographs in (A to D). The images are at the depth of the epidermal layer. Dots correspond to CL. Colour shift from red or yellow to green indicates an increasing proportion of high frequency content within the ultrasound signal emanating from smaller microvessels. **(I to L)** Cross-sectional UB-RSOM 2G images corresponding to the white dotted rectangles in the clinical photographs in (a)-(d). The tips of the

CL appear as dots while the perpendicular sections of the loops cannot be imaged and appear as black areas. Mean capillary loop length, MCLL; mean plexus width (mean width of the SVP), MPW. Scale bars 250 μm. **(M)** Local PASI during treatment. **(N)** MPW. **(O)** mean capillary loop diameter (MCLD), and **(P)** MCLL. **(Q to R)** Clinical imaging of psoriatic skin of a patient undergoing biologics treatment. Visual inspection on weeks 4 and 5 of treatment revealed no pathology and consequently the PASI index value was graded zero. **(S to T)** UB-RSOM 2G imaging of affected skin (white dashed rectangles) in (Q to R). (**U to W)** Local PASI index, MCLL, and MPW of skin in (Q, R). Scale bars: 200 μm.

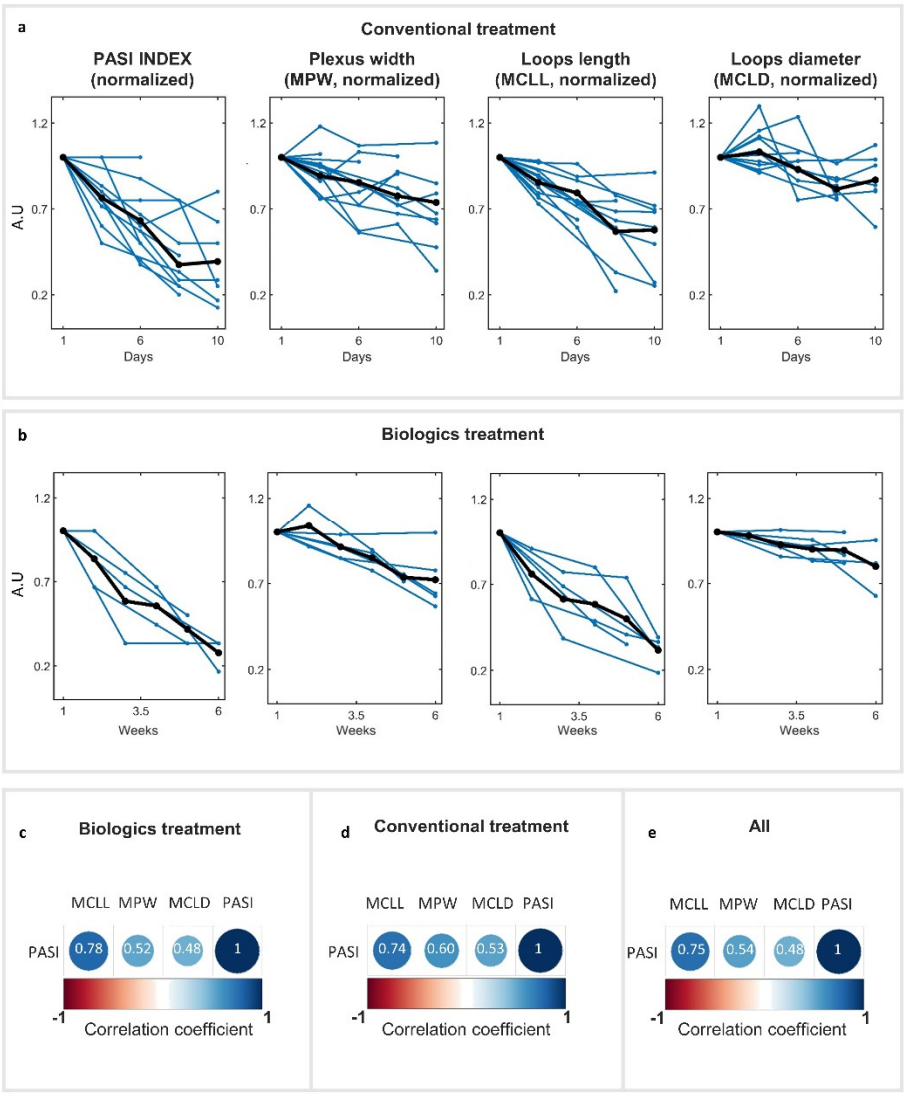

Fig. 3. **Change in UB-RSOM 2G biomarkers during psoriasis treatment. (A)** The evolution of each of the RSOM features (biomarkers) over time for patients receiving conventional treatment. Blue lines represent each individual patient and black lines the average. **(B)** Each graph shows the evolution of each RSOM biomarkers as function of the biologics treatment time. **(C)** Correlation coefficients between PASI and the RSOM biomarkers calculated for the patients undergoing biologics treatment. **(D)** Correlation coefficients between PASI and the RSOM biomarkers calculated for the patients undergoing conventional treatment. (**E**) Correlation coefficients between PASI and the RSOM biomarkers calculated for all patients.

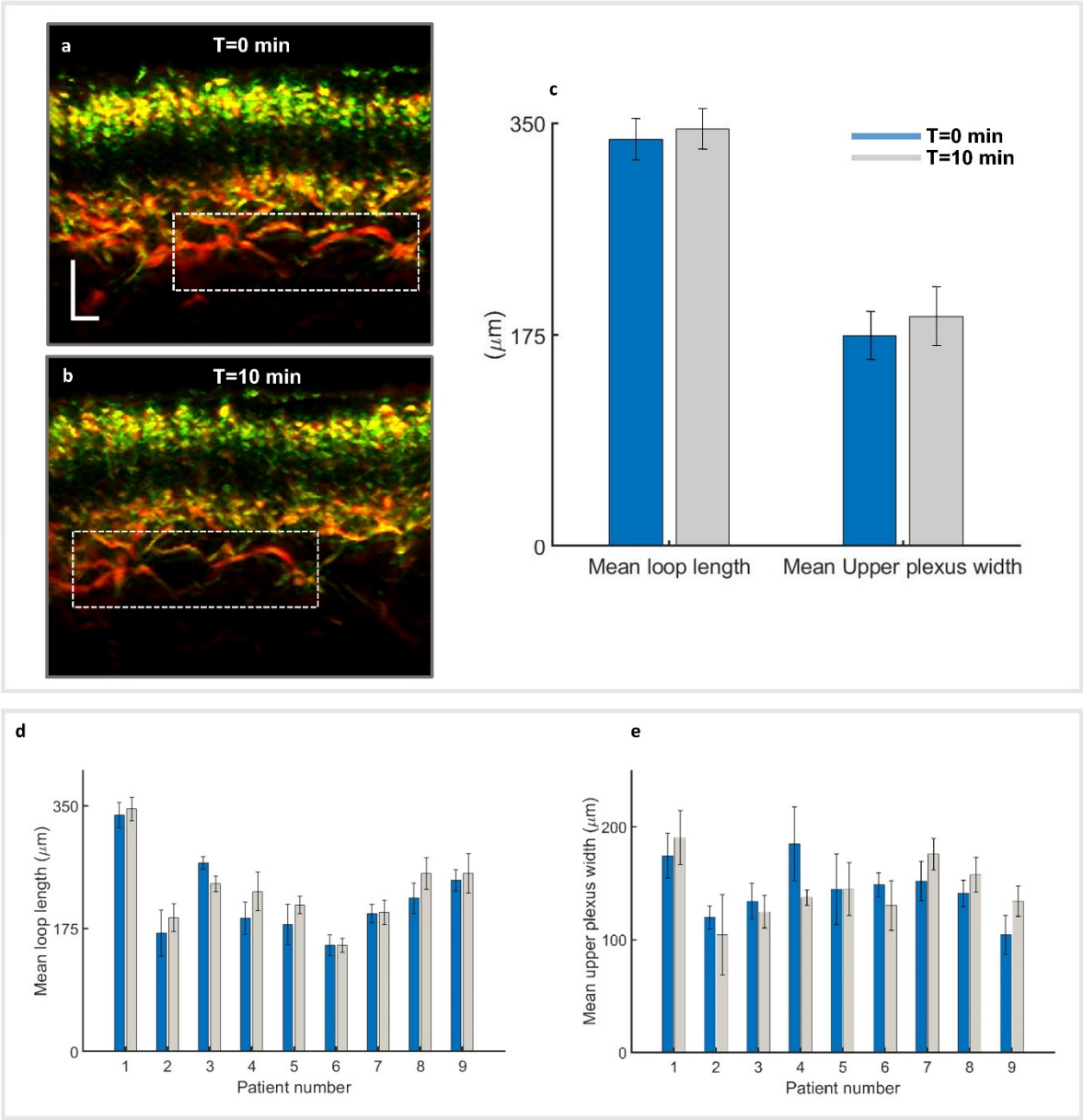

Fig. 4. **Repeatability of biomarkers extracted from UB-RSOM 2G measurements. (A** and **B)** Sample images for one patient from the repeatability study. An initial image was recorded (t=0) followed by a second image after 10 minutes (t=10). The dashed rectangle shows the same structure in both images. It can be observed that the scan head could not be placed at the identical position in both measurements. The positioning error was about 900 µm. (**C**) Values of the MCLL and MPW corresponding to images (A) and (B). The measurement could be repeated within a difference of a few tens of micrometers. (**D**) Values of the MCLL calculated from both measurements (t=0 and t=10 min) for each patient. (**E**) Values of the MPW calculated from both measurements (t=0 and t=10 min) for each patient. Scale bars: 200 µm.

Supplementary Materials

Materials and Methods

Technique for imaging precisely the same region of a psoriatic plaque over time

To ensure that potential changes could be monitored in precisely the same skin area we developed a protocol based on ink fiducial markers and the UB-RSOM 2G system's detachable interface unit in patients undergoing conventional treatment. The protocol included defining a Region of Interest (ROI) marking two green ink dots separated by a gap of 4 mm, a distance that corresponded to UB-RSOM's transversal field-of-view. For each imaging session, the scan head was positioned with care, ensuring that the ink dots were placed at the limits of the field-of-view and in the centre of its coronal axis (fig. S1A). After filling the interface with water, fast pre-acquisitions allowed us to localize the ink markings (fig. S1B) in the optoacoustic sinogram and, based on these markings, adjust the position of the scan area by modifying the home position of the UB-RSOM's motorized stages.

This protocol could only be applied in the patients undergoing conventional inpatient treatment as in the biologics group the time span between two examination time points was too long to maintain the fiducial markers at the same location. In those patients, photographs were used to ensure that the imaged part of the monitored psoriatic plaque remained as similar as possible.

Extraction of the RSOM biomarkers

RSOM biomarkers are extracted from reconstructed data. The first step in the extraction process is to flatten the surface of the skin from 3D images. Flattening allows to calculate the biomarkers in a simple form from cross sectional 2D MIPs. If flattening is not performed, epidermal and dermal structure would overlap in the MIP views preventing for measuring biologically meaningful parameters. For such flattening, it is mandatory to identify the skin surface, which is done by manually selecting 10 surface points from 20 µm thick MIPs in the y-direction (fig. S4a). Once this is done for every MIP of the 3D volume, the whole 3D skin surface can be interpolated and then flattened simply by performing rigid translations of every column of voxels in the z-direction. Then, the MCLL, MPW and MCLD are calculated from the MIP (fig. S4b,c). The MCLL is calculated by manually placing a segment in the z-direction that connects the upper edge of the microvascular plexus with the tip of the capillary loops closest to the skin surface. Then, the length is computed. The process is performed 7 times along the x-axis and the mean value is calculated (see blue arrows in Fig. S4). A similar operation is performed to calculate the MPW. Now the segment covers the entire vascular plexus (see white arrows in Fig. S4). The MCLD is computed by selecting randomly 10 tips of capillary loops and calculating their diameter as the full width half maximum of a profile the axial direction. All the biomarker measurements were performed using routines programmed in Matlab.

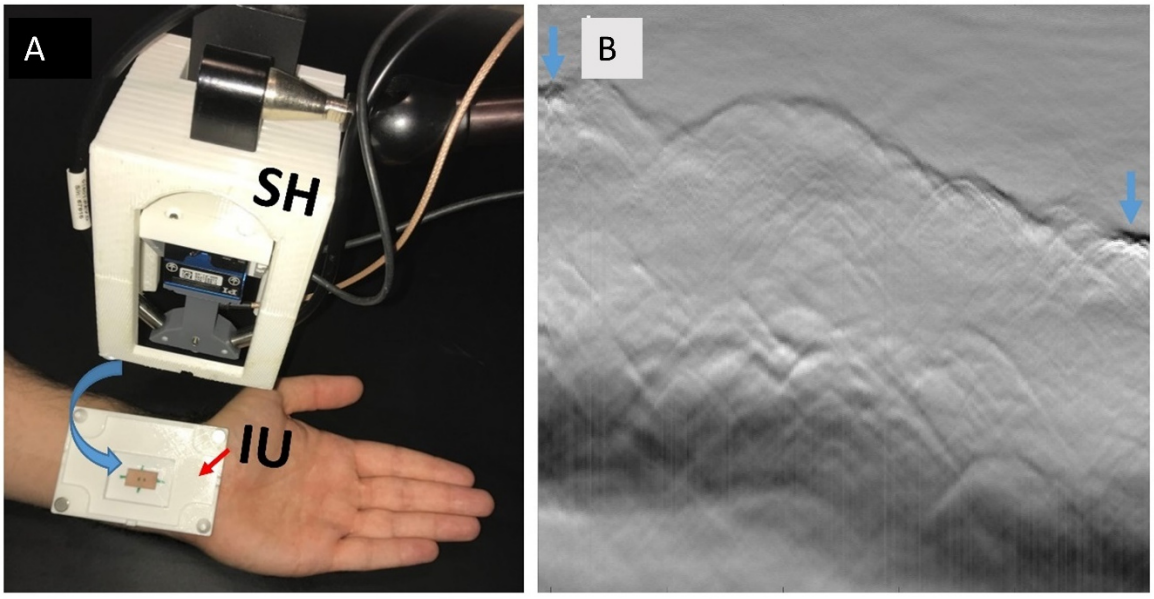

Fig. S1. Technique for imaging precisely the same region of a psoriatic plaque over time. (**A**) The transversal limits of the skin area to be imaged are marked with ink fiducial markers (two dark green dots, red arrow) which are preserved for the entire time of the study participation. The detachable interface unit (IU) is subsequently placed according to the fiducial markers. After the scan head (SH) has been attached to the interface unit (blue arrow), the interface unit is filled with water before scanning. The fiducial markers are visualized in the optoacoustic sinogram (**B**, blue arrows) and used to further modify the home position of the scanning head to precisely adjust the scan area.

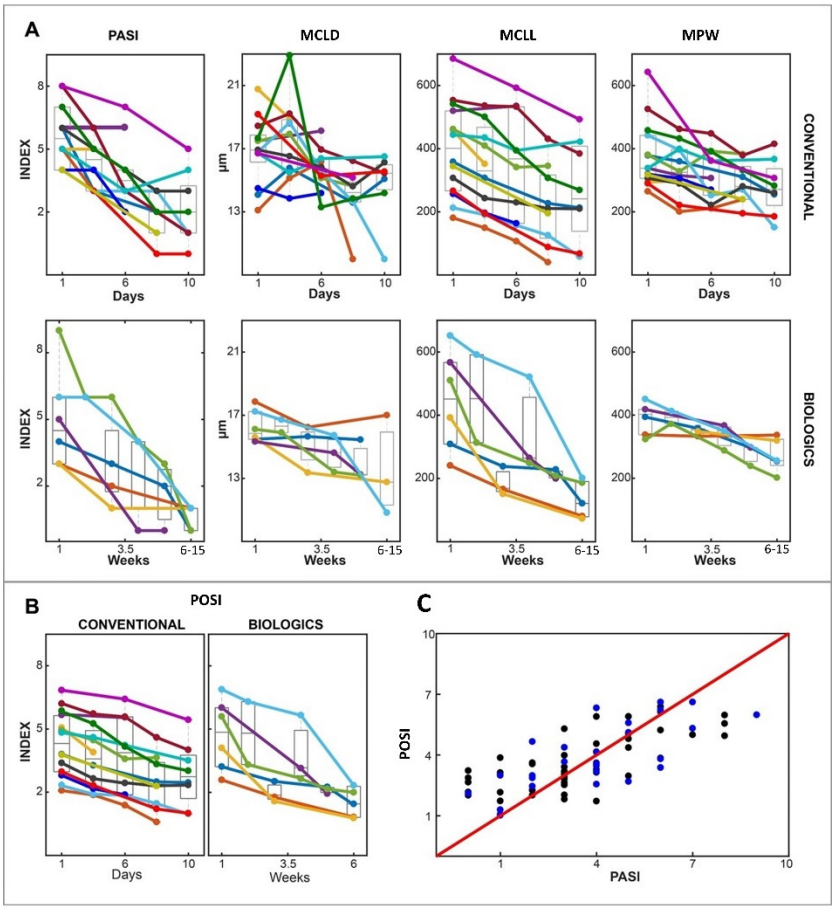

Fig. S2. Change in UB-RSOM 2G biomarkers during psoriasis treatment and optoacoustic severity index (POSI). (**A**) Absolute values of local PASI and corresponding measurements of optoacoustic biomarkers. Each graph shows the evolution of each of the RSOM biomarkers (MCLD Mean capillary loop diameter, MCLL Mean capillary loop length, MPW Mean plexus width) as function of the conventional and biologics treatment time in absolute values. Each color represents an individual patient. (**B**) The graphs show the evolution of the psoriasis optoacoustic severity index (POSI) during conventional and biologics treatment as a function of time. POSI combines the severity metrics of the MPW and the MCLL. Each color represents an individual patient. (**C**) Regression analysis of POSI and local PASI. MPW and MCLL showed good correlation with the local PASI (Pearson correlation coefficient corr=0.69 and corr=0.74, respectively). The POSI showed excellent correlation with local PASI (r^2=0.77, P = 0.00004)

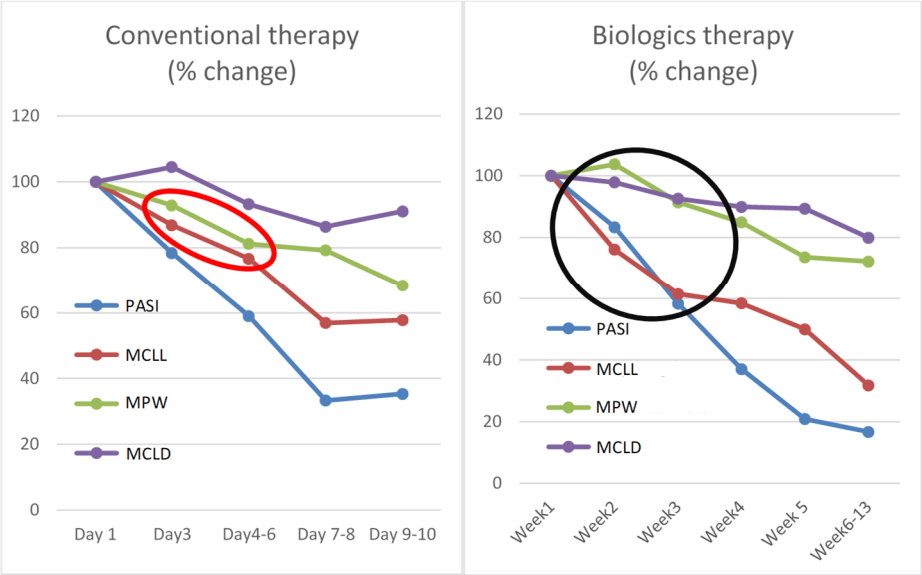

Fig. S3. Mean percent change of PASI and optoacoustic biomarkers. Changes of local PASI and biomarkers extracted from psoriatic plaques between day 1 and day 9 or 10 of conventional therapy (left) and between week 1 and weeks 6 to 13 during biologic therapy (right). During the early phases of conventional treatment the UWB RSOM 2G biomarkers, in particular MCLL and MPW, drop at a much more similar rate (red circle) than during the early phases of biologics treatment (black circle).

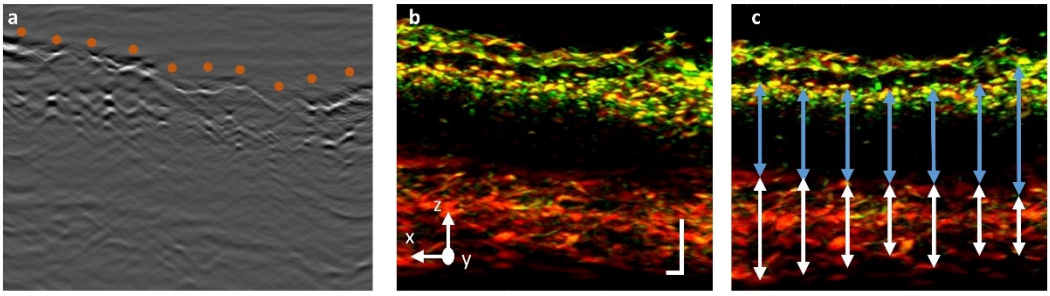

Fig. S4. Technique for computing biomarkers in reference to the skin surface. (**A**) Manual selection of points on the skin surface. The orange spheres represent the surface points manually selected for skin flattening. (**B**) Reconstructed RSOM image. (**C**) The image retains information on the skin surface from (A) so that all metrics are computed in reference to the skin surface. Scale bars: 250 µm. The MCLL is calculated by manually placing a segment in the z-direction that connects the upper edge of the microvascular plexus with the tip of the capillary loops closest to the skin surface. Then, the length is computed. The process is performed 7 times along the x-axis and the mean value is calculated (blue arrows). A similar operation is performed to calculate the MPW, where the segment covers the entire vascular plexus (white arrows). The MCLD is computed by selecting randomly 10 tips of capillary loops and calculating their diameter as the full width half maximum of a profile the axial direction.

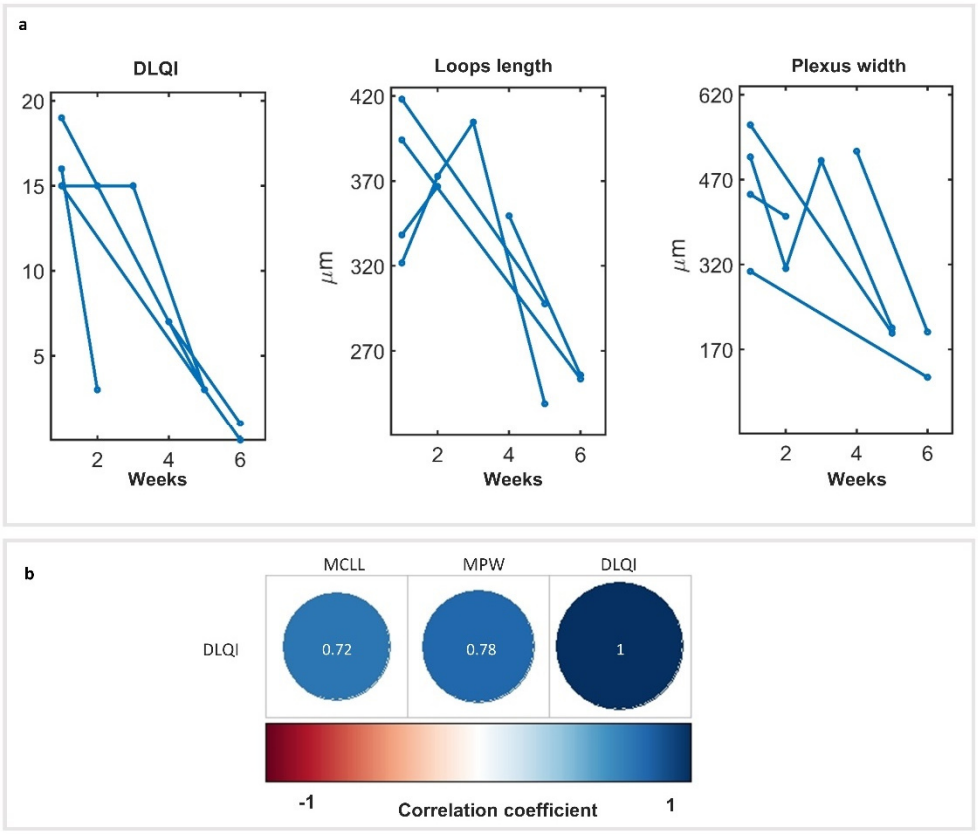

Fig. S5. **Correlation between the DLQI and the RSOM biomarkers.** (**A)** Evolution of the DLQI, loop length and plexus width as function treatment time for several patients. (**B)** Pearsons correlation coefficient between the DLQI and MPW and between the DLQI and MCLL values. There is a significant positive correlation both for the MCLL (Pearson correlation coefficient 0.72, P = 0.008) and the MPW (Pearson correlation coefficient 0.78, P = 0.003). DLQI data was available for 5 patients, most of them treated with biologics therapy.